Biophysical Characterization of the Enzyme I of the *Streptomyces coelicolor* Phosphoenolpyruvate:Sugar Phosphotransferase System

Estefanía Hurtado-Gómez,* Gregorio Fernández-Ballester,* Harald Nothaft,† Javier Gómez,* Fritz Titgemeyer,† and José Luis Neira*‡

*Instituto de Biología Molecular y Celular, Universidad Miguel Hernández, Alicante, Spain; †Lehrstuhl für Mikrobiologies, Friedrich-Alexander-Universität Erlangen-Nürnberg, Erlangen, Germany; and ‡Biocomputation and Complex Systems Physics Institute, Zaragoza, Spain

ABSTRACT The first protein in the bacterial phosphoenolpyruvate (PEP):sugar phosphotransferase system is the homodimeric 60-kDa enzyme I (EI), which autophosphorylates in the presence of PEP and Mg^{2+}. The conformational stability and structure of the EI from *Streptomyces coelicolor*, EI^{sc}, were explored in the absence and in the presence of its effectors by using several biophysical probes (namely, fluorescence, far-ultraviolet circular dichroism, Fourier transform infrared spectroscopy (FTIR), and differential scanning calorimetry) and computational approaches. The structure of EI^{sc} was obtained by homology modeling of the isolated N- and C-terminal domains of other EI proteins. The experimental results indicate that at physiological pH, the dimeric EI^{sc} had a well-folded structure; however, at low pH, EI^{sc} showed a partially unfolded state with the features of a molten globule, as suggested by fluorescence, far-ultraviolet circular dichroism, FTIR, and 8-anilino-1-naphthalene-sulfonic acid binding. The thermal stability of EI^{sc}, in the absence of PEP and Mg^{2+}, was maximal at pH 7. The presence of PEP and Mg^{2+} did not change substantially the secondary structure of the protein, as indicated by FTIR measurements. However, quenching experiments and proteolysis patterns suggest conformational changes in the presence of PEP; furthermore, the thermal stability of EI^{sc} was modified depending on the effector added. Our approach suggests that thermodynamical analysis might reveal subtle conformational changes.

INTRODUCTION

The bacterial phosphoenolpyruvate-dependent sugar phosphotransferase system (PTS) is a multiprotein complex system that phosphorylates and, concomitantly, transports carbohydrates across the membrane into the cell (1). The PTS involves a cascade of phosphoryl-transfer steps from phosphoenolpyruvate (PEP) via phosphointermediates of the general cytosolic non-sugar-specific phosphotransferases enzyme I (EI) and the histidine-phosphocarrier (HPr) to sugar-specific enzyme II permeases. EI is autophosphorylated on a histidine residue by PEP in the presence of Mg^{2+}, and the phosphoryl group is then transferred to HPr (1). The activity of EI is regulated by a monomer-dimer equilibrium, where the autophosphorylation requires the dimeric species (2–4). Although in a system as complex as the PTS, it is likely that more than one form of regulation must exist, the existence of the monomer-dimer equilibrium and the non-sugar specificity of EI make this protein an excellent target to control different cellular functions (such as transport and chemotaxis) (5) and to understand the protein-protein interactions in the PTS.

EI proteins are composed of two domains (6,7): a proteolytically inert N-terminal (EIN), and a proteolytically unstable C-terminal domain (EIC). The isolated EIN is a monomer, which cannot be phosphorylated by PEP, but participates in a reversible phosphorylation reaction with phosphorylated HPr (2,6). The structure of EIN from *Escherichia coli* has been solved by x-ray (8) and NMR (9), and its complex with HPr has been described by NMR (10). EIN is composed of an HPr-binding α-helical subdomain and an α/β subdomain containing the active site histidine. On the other hand, the EIC domain contains the PEP-binding region and the dimerization interface, as shown by the crystal structure of the EIC from *Thermoanaerobacter tengcongensis* (11). The folding features of both domains are different. EIN shows a reversible thermal two-state transition; whereas EIC has a broad-scan-rate, concentration-dependent thermal transition (2,12). Since the folding process is complex in multidomain proteins, where each domain may be able to refold independently and interdomain interactions may affect the overall folding process, EI can be used, in addition, as a model protein to improve our knowledge of protein folding and assembly of multidomain-oligomeric proteins.

Streptomyces are soil-dwelling actinomycetes which grow on a vast variety of carbon sources, such as mono- and disaccharides, as well as the most abundant biopolymers on Earth (cellulose, chitin, and xylan). These actinomycetes are the origin of approximately two-thirds of all natural antibiotics currently produced by the pharmaceutical industry. The complete genome of *Streptomyces coelicolor* has been sequenced, and it shows the largest number of genes found in any bacterium (13). The presence of the different components of the PTS in *S. coelicolor* has been reported, and the corresponding proteins cloned and expressed (14–16).

Submitted October 31, 2005, and accepted for publication March 7, 2006.

Address reprints requests to José L. Neira, Instituto de Biología Molecular y Celular, Edificio Torregaitán, Universidad Miguel Hernández, Avda. del Ferrocarril s/n, 03202, Elche (Alicante), Spain. Tel.: 34-966658459; Fax: 34-966658758; E-mail: jlneira@umh.es.

0006-3495/06/06/4592/13 $2.00

doi: 10.1529/biophysj.105.076935

Although there is a wealth of information on the PTS in Gram-negative and low-G+C Gram-positive bacteria, information on PTS proteins present in high-G+C Gram-positive bacteria is very limited. We have undertaken an extensive description of the structures and conformational stabilities of the PTS proteins of *S. coelicolor*, first, to understand in depth the mechanism of the PTS; and, second, to provide new clues on the protein folding problem. For instance, we have shown that the thermodynamic folding parameters (ΔC_p and *m*-values) of the HPr of *S. coelicolor*, HPr^{sc}, are different from those of the other members of the HPr family (17–19). Interestingly enough, HPr^{sc}, in contrast to the HPrs in Gram-negative bacteria and low-G+C Gram-positive bacteria (1), is not involved in general carbon regulation (20,21). Then, one is tempted to ask, is there any relationship among the different functions and structures of the PTS proteins on one side, and the thermodynamic parameters and folding properties on the other? To answer this question, it is necessary to describe the conformational preferences of proteins, where studies of different members of the family have been described. There is now increasing evidence that looking at the structure alone is not sufficient to answer these scientific questions (22). Rather, structures need to be associated to other bodies of data, putting them into specific biological context. Those other sets of data include folding classification, taxonomic identification, their role in metabolic routes, biophysical data, and conformational stability.

Preliminary Fourier transform infrared spectroscopy (FTIR) and circular dichroism (CD) thermal denaturations at physiological pH on the EI enzyme of *S. coelicolor*, EI^{sc}, indicate that its thermal denaturation behavior is different from that of other EI proteins, since only one transition is observed (23). In this work, we further investigate the stability and structure of EI^{sc} at different pH in the absence and in the presence of its effectors (PEP and Mg^{2+}), by using theoretical and experimental approaches. Our results show that dimeric EI^{sc} acquired a folded conformation at physiological pH; however, 8-anilino-1-naphthalene-sulfonic acid (ANS)-binding experiments, FTIR, and CD measurements suggested that the protein populated a molten-globule-like species at low pH. Further, we modeled the structure of EI^{sc}, by using the structures of the N-terminal domain of EI from *E. coli*, EIN^{ec} (9), and the C-terminal domain of *T. tengcongensis*, EIC^{tt} (11), as templates. This modeled structure has allowed us to explain the experimental conformational and thermodynamic features of the protein. Finally, we studied the conformational and stability properties of EI^{sc} in the presence of the effectors (i.e., Mg^{2+} and PEP). Our results show that the secondary structure of EI^{sc} was not substantially altered, as suggested by FTIR experiments, but quenching experiments and proteolysis patterns suggest that there were small conformational changes upon binding of PEP; in addition, the thermal stability of EI^{sc} was slightly modified when any effector was added. In conclusion, our approach suggests that thermodynamical analysis might reveal subtle conformational changes in otherwise similar folds.

MATERIALS AND METHODS

Materials

Imidazole, the different salts and acids used in buffer preparation, sodium pyruvate, and NaCl were from Sigma (St. Louis, MO). The β-mercaptoethanol was from BioRad (Hercules, CA), and the Ni^{2+}-resin was from Invitrogen (Carlsbad, CA). Standard suppliers were used for all other chemicals. Water was doubly deionized and purified on a Millipore (Billerica, MA) system. The trypsin proteomics grade was from Sigma.

Protein expression and purification

The EI^{sc} clone comprises residues 1–576, with an extra methionine and a His_6-tag at the N-terminus (15). The protein was expressed and purified as described (23). Protein was >95% pure as judged by sodium dodecyl sulfate polyacrylamide gel electrophoresis (SDS-PAGE). EI^{sc} was dephosphorylated by overnight dialysis at 278 K against phosphate potassium buffer (10 mM, pH 7.5), 10 mM sodium pyruvate, 1 mM $MgCl_2$, followed by extensive dialysis against the same buffer in the absence of $MgCl_2$ and pyruvate. Samples were frozen in liquid nitrogen and stored at –80°C. Protein concentration was calculated by using the extinction coefficients of Trp, Tyr, Cys, and Phe residues (24). The yield of the protein was 5–8 mg per liter of culture.

CD measurements in the far-ultraviolet (UV) region

Spectra were collected on a Jasco J810 (Tokyo, Japan) spectropolarimeter fitted with a thermostated cell holder and interfaced with a Peltier cell, working at 298 K. The instrument was periodically calibrated with (+) 10-camphorsulphonic acid. The final concentrations were 5 mM $MgCl_2$ and 2.5 mM PEP. The mean residue ellipticity, $[\Theta]$, was obtained from the raw ellipticity data, Θ, as described (23), and all spectra were corrected with the proper baseline.

In the pH-denaturant experiments followed either by CD or fluorescence (see below), the pH was measured before and after completion of experiments with an ultrathin Aldrich electrode in a Radiometer pH-meter (Copenhagen, Denmark). Three-point calibration of the pH-meter was performed by using standards from Radiometer. The salts and acids used in buffer preparation were: phosphoric acid, pH 2.0–3.0; formic acid, pH 3.0–4.0; acetic acid, pH 4.0–5.5; monosodium dihydrogen phosphate, pH 6.0–7.0; Tris basic, pH 7.5–9.0; sodium carbonate, pH 9.5–11.0; and sodium phosphate, pH 11.5–13.0.

Steady-state measurements

Spectra were acquired in a 0.1-cm-pathlength cell with a speed of 50 nm/min and a response time of 4 s, and were averaged over four scans. Protein concentration was 4 μM.

Thermal denaturation measurements

Experiments were performed with a response time of 8 s and at constant heating rates of 15, 30, and 60 K/h to test for microreversibility (6), in the presence of 1 mM β-mercaptoethanol. No variations in the T_m were observed among the three scan rates, and thus, the criterion for microreversibility was satisfied. Measurements were acquired every 0.2 K. Thermal scans were followed by changes in the ellipticity at 222 nm from

298 to 353 K. The reversibility of thermal transitions was tested by recording a new scan after cooling the thermally denatured sample to 298 K, and comparing the thermal denaturation curve with that obtained in the first scan.

Fluorescence measurements

Fluorescence spectra were collected in a Cary Eclipse spectrofluorometer (Varian, San Carlos, CA) interfaced with a Peltier cell. A 1-cm-pathlength quartz cell (Hellma, Muellheim/Baden, Germany) was used. The slit widths were 5 nm for the excitation and emission wavelengths. Protein concentration was 4 μM, unless otherwise indicated. Steady-state and quenching experiments were acquired at 298 K.

Steady-state intrinsic fluorescence

Protein samples were excited at 280 and 295 nm between pH 2–12. Experiments were recorded between 300 and 400 nm. The signal was acquired every second, and the increment of wavelength was set to 1 nm. Blank corrections were made in all spectra.

Steady-state ANS binding

ANS binding was detected by collecting fluorescence spectra at different pH in the presence of 100 μM of dye. Excitation wavelength was 370 nm, and the emission intensity was collected from 430 to 700 nm. Stock solutions of ANS were prepared in water by using a molar extinction coefficient of 6.8×10^3 M^{-1} cm^{-1} at 370 nm (25). Blank corrections were made in all spectra.

Quenching experiments

Quenching of intrinsic tryptophan and tyrosine fluorescence by either iodide or acrylamide was examined at different pH values, by excitation at 280 and 295 nm. In the experiments employing KI as a quencher, ionic strength was kept constant by addition of KCl; $Na_2S_2O_3$ was added to a final concentration of 0.1 M to avoid formation of I_3^-. The dynamic and static quenching constants were obtained by fitting the fluorescence intensity at 338 nm to the Stern-Volmer equation, which includes an exponential term to account for static quenching (26):

$$F_0/F = (1 + K_{sv}[X])e^{(\upsilon[X])}, \quad (1)$$

where K_{sv} is the Stern-Volmer constant for collisional quenching, υ is the static quenching constant, F_0 is the fluorescence in the absence of quencher, and $[X]$ is the concentration of the quencher. The range of quencher concentrations was 0–0.7 M. Iodide quenching did not show a significant static component, and then the exponential term was not included.

In experiments aimed to detect protein self-association, the concentration of EI^{sc} was varied at pH 7 from 0.5 to 4 μM, and only KI was used as the quencher.

In experiments aimed at detecting the burial of the aromatic residues upon binding to PEP and/or Mg^{2+}, the concentration of EI^{sc} was 4 μM at pH 7.0, and only acrylamide was used as quencher. Concentrations of effectors were 2.5 mM of PEP and 5 mM of Mg^{2+}. Experiments were only carried out at 280 nm, where the signal/noise ratio of the Stern-Volmer plots was higher.

Thermal denaturation measurements

Thermal unfolding curves were determined in the presence of 1 mM β-mercaptoethanol by following the emission fluorescence at 315, 335, or 350 nm, after excitation at 280 and 295 nm, with a scan rate of 30 K/h. The three wavelengths yielded the same unfolding curves (data not shown).

Thermal denaturation experiments were also carried out by following the emission fluorescence of ANS either at 480 or 520 nm, after excitation at 360, 380, or 390 nm, at three different pH, 2.0, 3.5, and 8.0 The scan rates were 30 K/h.

Trypsin digestion experiments

EI^{sc} was mixed with trypsin (at final concentrations of 1 μg/μl for EI^{sc} and 0.002 μg/μl for trypsin, that is, the final concentration rate between both proteins was 500:1) in a total volume of 17 μl in 100 mM of Tris buffer at pH 7 (27). Lower concentration rates of protein to trypsin were used (100:1, 200:1, and 300:1), but in all these experiments the amount of nondigested EI^{sc} in the absence of effectors was insignificant after 1 min of reaction (data not shown). Samples were incubated at 25°C for 10 min. Digestion was stopped by the addition of 17 μl of SDS-PAGE loading buffer, and samples were immediately run on a gel. The intensities of the bands at different times were measured by densitometry. Experiments were carried out in the absence and in the presence of the effectors (at final concentrations of 2.5 mM PEP and 5 mM Mg^{2+}), and every digestion was repeated three times.

Differential scanning calorimetry

Differential scanning calorimetry (DSC) experiments were performed with a VP-DSC differential scanning calorimeter (MicroCal, Northampton, MA) by using a protein concentration of 1.27 mg/ml (~20 μM). Protein was extensively dialyzed against 2 L of the working buffer (5 mM HEPES buffer containing 10 mM NaCl and 2 mM β-mercaptoethanol, pH 7) at 278 K. In experiments with the effectors (5 mM Mg^{2+} and 2.5 mM PEP), the dialyzed protein solution was supplemented with such effectors taken from a stock solution freshly prepared in the same buffer. The sample with the protein and the effectors was incubated for a minimum of 2 h at room temperature. Samples were degassed under vacuum for 10–15 min with gentle stirring before being loaded into the calorimetric cell. DSC experiments were performed under a constant external pressure of 30 psi to avoid bubble formation and samples were heated at a constant scan rate of 60 K/h. Once the first scan was completed, the samples were cooled down in situ to 283 K for 15 min and rescanned under the same experimental conditions to test for the reversibility of the denaturation reaction. Calorimetric denaturations were reversible in all cases. Experimental data were corrected from small mismatches between the two cells by subtracting the buffer baseline before data analysis. Once thermograms were normalized to protein concentration, a chemical baseline calculated from the progress of the unfolding transition was subtracted. For experiments involving PEP, control scans were acquired with PEP added to buffer versus buffer in the reference cell, and baselines were found to be the same as in buffer-buffer baselines, suggesting that under these conditions hydrolysis of PEP during heating was not significant. The excess heat capacity functions were then analyzed using the software package Origin 7.0 (Microcal). The best fit was obtained by using the two-state model.

FTIR

The protein was speed-vacuum dried (Speed-vac rotatory evaporator, Savant Instruments, Farmingdale, NY) and dissolved in the deuterated buffer containing 100 mM NaCl. Protein was still functional after the concentration step, as shown by binding experiments (28). No pH corrections were done for the isotope effects. Samples of EI^{sc} at a final concentration of 44.7 mg/ml (~1 mM) were placed between a pair of CaF_2 windows separated by a 50-μm-thick spacer in a Harrick demountable cell. Spectra were acquired on a Bruker (Madison, WI) FTIR instrument equipped with a deuterated triglycine sulfate detector and thermostated with a Braun (Kronberg, Germany) water bath. The cell holder was continuously filled with dry air. When effectors were added, the final concentrations were 5 mM $MgCl_2$ and 2.5 mM PEP at pH 7.

Steady-state measurements

Three-hundred scans per sample were taken, averaged, apodized with a Happ-Genzel function, and Fourier transformed to give a final resolution of 2 cm^{-1}. The signal/noise ratio of the spectra was better than 1000:1. Buffer

contributions were subtracted, and the resulting spectra were used for analysis. To quantify the secondary structure components, the amide I′ band was decomposed into its constituents by curve-fitting (based on a combination of Gaussian and Lorentzian functions). The number and position of bands obtained from the deconvoluted (with a Lorentzian bandwidth of 18 cm^{-1} and a resolution enhancement factor of 2) and the Fourier derivative (with a power of 3 and a breakpoint of 0.3) of the spectra (29–31) were used for analysis of the percentages of secondary structure. The experiments recorded at 298 K, and acquired at pH 3.0, 7.0, 8.5, and 10.0. Experiments between pH 4 and 5.5, where an acidic titration was observed (see Results), could not be carried out since the acetic moiety used in the buffer absorbs strongly in the amide I′ region of the infrared spectrum.

Thermal denaturation measurements

Thermal denaturation experiments were carried out with a scanning rate of 50 K/h, and acquired every 3 K. Fifty scans per temperature were acquired and averaged.

Analysis of the pH- and thermal-denaturation curves

The pH-denaturation experiments were analyzed assuming that both species, protonated and deprotonated, contributed equally to the fluorescence intensity, Y:

$$Y = \left(Y_a + Y_b 10^{n(pH-pK_a)}\right) / \left(1 + 10^{n(pH-pK_a)}\right), \quad (2)$$

where n is the Hill coefficient, which gives a measurement of the cooperativity of the transition, and the number of residues involved in the titration; Y_a is the fluorescence at low pHs; Y_b is the fluorescence at high pH; and pK_a is the apparent midpoint of the sigmoidal curve.

Thermal-denaturation parameters were obtained by following the change in the physical property, Y (the fluorescence intensity, the Θ and the half-height width of the amide I′ band of the FTIR experiments), to:

$$Y = \left(Y_N + Y_D e^{(-\Delta G/RT)}\right) / \left(1 + e^{(-\Delta G/RT)}\right), \quad (3)$$

where $Y_N = \alpha_N + \beta_N[D]$ and $Y_D = \alpha_D + \beta_D[D]$ are the baselines of the folded and unfolded states, respectively, for which a linear relationship with denaturant is assumed; R is the gas constant; and T is the temperature in K.

The change in free energy is given by (32):

$$\Delta G(T) = \Delta H_m\left(1 - \frac{T}{T_m}\right) - \Delta C_p\left[(T_m - T) + T\ln\left(\frac{T}{T_m}\right)\right] - RT\ln(2C_t), \quad (4)$$

where ΔH_m is the van't Hoff enthalpy change, T_m is the midpoint of the thermal denaturation, ΔC_p is the heat capacity change, and C_t is the total molar concentration of the protein expressed in dimer equivalents.

The fittings to Eqs. 2–4 were carried out by using the general curve-fit option of Kaleidagraph (Abelbeck software) working on a PC computer.

Modeling of the EI^{sc} structure

The structures of the N- and C-terminal domains of *S. coelicolor* were obtained by homology modeling. Sequence alignments between species were made with CLUSTALW at the EBI website (http://www.ebi.ac.uk) by using the Needleman-Wunsch global alignment algorithm (with the following parameters: matrix: EBLOSUM62, gap penalty value: 10.0, extended penalty value: 5.0) to find the optimum alignment (a 40% identity and a 52% similarity).

The models were constructed with the SWISS MODEL server (33) by using the structures of EIN^{ec} (PDB accession code 1ZYM) and EIC^{tt} (PDB accession code 2BG5) as templates. The orientation and optimization of side chains were carried out in two steps. Firstly, those residues making van der Waals clashes were selected and fitted with ''Quick and Dirty'' algorithms; and secondly, models were energy minimized (100 steps of steepest descent and 100 conjugate gradients, with a cut-off of 10 Å for nonbonded interactions) with Insight II (Biosym/MSI). Structure edition was made with Swiss PDB viewer v3.7 (34) and Insight II. The model was tested in terms of energy with Fold-X (http://foldx.embl.de) (35,36) which evaluates the properties of the structure, such as the atomic contact map, the accessibility of atoms and residues, the backbone dihedral angles, and the hydrogen bond and electrostatic networks of the protein. Fold-X was also used to evaluate the interaction energy in the dimer formed by both C-terminal domains by calculating the difference in stability energy between the dimer and the isolated domains. Further, the model was evaluated with PROCHECK (37), showing a Ramachandran plot with 89.1% of the residues in the most favorable regions and 10.3% in additional generously allowed regions. Molecular graphics were created with PyMOL (38).

RESULTS

Structure and stability of EI^{sc} in the absence of effectors

We carried out KI quenching experiments at different protein concentrations to test whether 1), self-association of EI^{sc} could be mapped by some of its fluorescence residues (one tryptophan and eight tyrosine residues); and, 2), we were able to estimate the self-association constant. We observed that at physiological pH as the concentration of protein was increased, the value of K_{sv} was reduced: 1.4 ± 0.1 at 0.5 μM, 0.94 ± 0.05 at 1 μM, 0.90 ± 0.03 at 2 μM, and 0.8 ± 0.1 at 4 μM of EI^{sc}. Those findings suggest that 1), EI^{sc} self-associates, as other EI proteins do (2–4); 2), fluorescent residues are involved in the self-association interface; and, 3), the value of 1 μM could be considered an upper estimation of the EI^{sc} self-dissociation constant.

Then, the experiments monitoring protein stability under different conditions were carried out at protein concentrations ≥4 μM.

pH-induced structural changes

Steady-state intrinsic fluorescence measurements. Fluorescence spectroscopy reports the changes in the tertiary structure of a protein (26). The emission fluorescence spectrum of EI^{sc}, by excitation at either 280 or 295 nm, showed a maximum at 335 nm, and thus, it was dominated by the emission of the sole tryptophan residue, Trp^{461}. The changes in the fluorescence intensity at 335 nm, at both excitation wavelengths, showed a bell-shaped profile, with a maximum at neutral pH (Fig. 1 *A*, *open squares*). At acidic pH, a sigmoidal curve with a pK_a of 4.3 ± 0.6 and n = 1.4 ± 0.3 was observed. The large fitting errors are probably due to the steepness of the experimental data between pH 5 and 6.

ANS-binding experiments. ANS-binding was used to monitor the extent of exposure of protein hydrophobic regions. When ANS binds to solvent-exposed hydrophobic patches, its quantum yield is enhanced and the maximum of emission is shifted from 520 nm to 480 nm (39,40). In EI^{sc} at

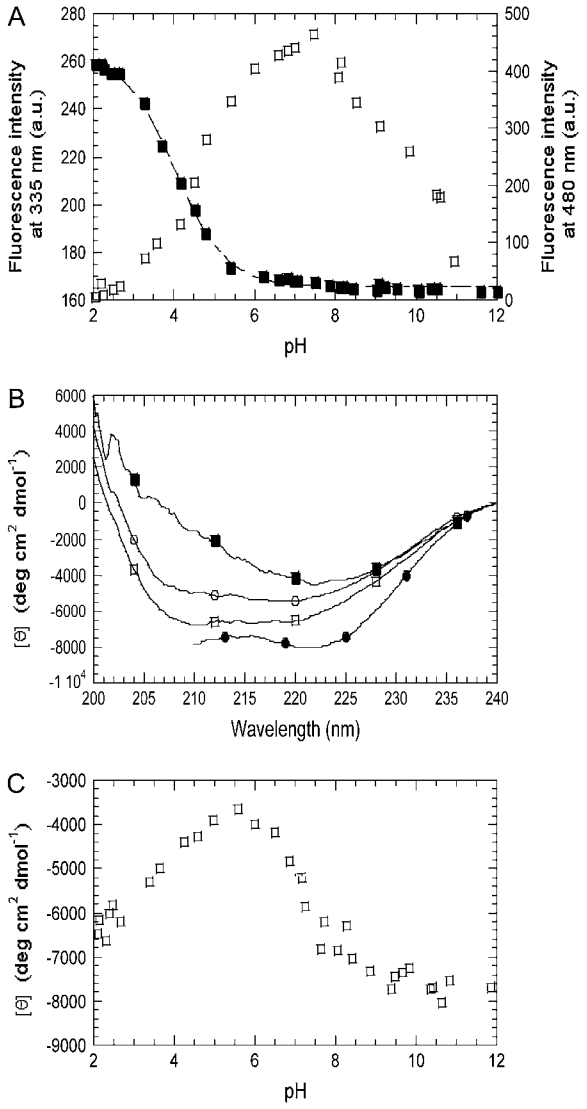

FIGURE 1 pH-induced unfolding of EI^{sc} in the absence of effectors followed by intrinsic fluorescence, ANS-binding, and far-UV CD. (*A*) The intrinsic fluorescence intensity at 335 nm obtained by excitation at 295 nm (*open squares*, *left axis*) and the ANS fluorescence at 480 nm (*solid squares*, *right axis*) versus pH. The line through the data of ANS is the fitting to Eq. 2. Dye concentration was 100 μM. (*B*) Far-UV CD spectra at selected pH: pH 2.1 (*open squares*); pH 4.1 (*solid squares*); pH 7.0 (*open circles*); and pH 10.5 (*solid circles*). (*C*) Changes in the molar ellipticity at 222 nm at different pH. Protein concentration was 4 μM. Experiments were acquired at 298 K.

low pH, the fluorescence intensity of ANS was largely enhanced, and the maximum wavelength of the fluorescence spectrum was 480 nm (Fig. 1 *A*, *solid squares*). As the pH was increased, the spectral intensity was reduced and the maximum wavelength was red-shifted toward 520 nm, following a sigmoidal behavior. From the changes in the fluorescence intensity, the apparent pK_a of the titration was 4.19 $\pm$ 0.07, with $n = 1.1 \pm 0.1$.

Fluorescence quenching. The solvent-accessibility of tryptophan and tyrosine residues was examined by iodide and acrylamide quenching at several pHs. Three pHs were chosen based on the steady-state fluorescence results: pH 5, close to the midpoint of the titration observed in ANS-binding and fluorescence intrinsic experiments; neutral pH, where the intensity of steady-state fluorescence experiments was at its maximum; and pH 12, in the basic region. Control experiments were carried out at 7 M GdmHCl, pH 7, where the protein was fully unfolded. Experiments at pH <4 led to sample precipitation.

Acrylamide quenching experiments, measured by excitation at either 280 or 295 nm, showed exponential Stern-Volmer plots (Table 1), which yielded similar results: the K_{sv} were larger at acidic than at neutral pH, and the experiments in GdmHCl had the largest values of K_{sv}. At basic pHs, the K_{sv}s were slightly larger than at neutral pH, but smaller than those at acidic pHs. The use of KI yielded similar results at both excitation wavelengths (Table 1): the values of K_{sv} were larger at acidic pHs and in GdmHCl than at neutral pH. At basic pHs, the K_{sv}s were similar, within the error, to those observed at pH 7.

In conclusion, the results from both quenchers suggest that at acidic pH, the aromatic residues became accessible to the solvent, although they were not as exposed as when EI^{sc} was fully unfolded (7 M GdmHCl). Further, partial solvent-exposure of fluorescent residues also occurred at basic pH.

Far-UV CD experiments. The far-UV CD spectrum of EI^{sc} at neutral pH showed the features of an α-helical protein with minima at 208 and 222 nm (41,42) (Fig. 1 *B*). This shape did not change as the pH was modified, except in the region between 3.0 to 5.5. In this pH range, the minimum at 208 nm disappeared, whereas that at 222 nm was still present. In the whole pH range explored, the absolute values of the [Θ] at 222 nm showed a bell-shaped tendency (Fig. 1 *C*), with a maximum shifted to lower pH (at pH 6) than that found in fluorescent experiments (Fig. 1 *A*, *open squares*). This could be due to the fact that CD is reporting global changes in the secondary structure, and fluorescence is monitoring the changes in tertiary structure around fluorescent residues.

FTIR experiments. At any of the explored pH, the percentages of β-hairpin (at 1693 cm^{-1}) turns/loops/(0, π) β-sheet (at 1679 cm^{-1}) and antiparallel β-sheet (at 1633 cm^{-1}) remained essentially unaltered. Conversely, at acidic pH, the percentage of β-turns appearing at 1668 cm^{-1} was decreased, and the percentages of helical structure, loops, and disordered structures (bands at 1648 and 1657 cm^{-1}, which could not be independently assigned at pH 3) were higher (50.9%) than those at neutral pH (pH 7 (44.5%) and 8.5 (40.3%)), but similar, within the error, to those observed at pH 10 (55%). These data suggest that the percentages of helical structure in EI^{sc} at the extremes of pH were increased.

Stability of EI^{sc} as monitored by DSC and thermal denaturations

From the spectroscopic results above, it can be concluded that EI^{sc} acquired a folded conformation around physiological

TABLE 1 Quenching constants for EI^{sc} in acrylamide and KI at 298 K

	Acrylamide				KI	
	280		295		280	295
Conditions	K_{sv} (M^{-1})	υ(M^{-1})	K_{sv} (M^{-1})	υ(M^{-1})	K_{sv} (M^{-1})	K_{sv} (M^{-1})
pH 5	5 ± 1	0.4 ± 0.2	3.9 ± 0.5	0.3 ± 0.1	1.3 ± 0.2	1.0 ± 0.1
pH 7	2.4 ± 0.2	1.0 ± 0.1	1.5 ± 0.2	0.6 ± 0.2	0.7 ± 0.1	0.6 ± 0.1
pH 12	3.5 ± 0.2	1.0 ± 0.1	2.7 ± 0.2	0.2 ± 0.1	0.8 ± 0.1	0.7 ± 0.1
7 M GdmHCl (pH 7)	7.0 ± 0.2	0.6 ± 0.1	4.6 ± 0.1	0.2 ± 0.1	2.9 ± 0.4	2.7 ± 0.4

Constants were obtained by fitting the fluorescence intensity data at 338 nm to Eq. 1. Errors are fitting errors.

pH, and that this structure was basically unaltered (except for changes in the ellipticity, Fig. 1 *C*) between pH 7 and 8. Since, EI^{sc} shows a sigmoidal thermal transition at neutral pH, with a $T_m = 330$ K (23), we can wonder whether there are sigmoidal thermal transitions at other pH, and if so, whether the T_ms are the same as at pH 7. To address these questions, we carried out calorimetric and thermal measurements by using DSC and several spectroscopic techniques (Table 3).

Fluorescence experiments. Thermal denaturations were carried out at pH 2, 3, 4, 7, 9, and 11. Fluorescence experiments at pH 7 and 9 showed a sigmoidal transition with $T_m = 311 \pm 4$ K (Fig. 2 *A*); this transition was more clearly observed when the protein was excited at 295 nm than when excited at 280 nm, suggesting that it was due to Trp^{461}. Since the tryptophan is at the C-terminus of EI^{sc}, the changes observed should reflect conformational rearrangements occurring in this region. Thermal denaturations at pH 2, 3, 4, and 11 did not yield a sigmoidal behavior (data not shown).

Thermal denaturations following the ANS fluorescence did not show a native baseline, and a sigmoidal-like decreasing of the fluorescence was observed as the temperature was raised (data not shown).

Far-UV CD experiments. Experiments were carried out at pH 2, 3, 4, 7, 9, and 11. In all cases, the absolute value of the ellipticity decreased linearly, as the temperature was raised. Sigmoidal transitions were only observed at pH 7 (23) and 9, with T_m close to 330 K (Fig. 2 *B*).

DSC experiments. Experiments were carried out at pH 4, 7, and 10. At pH 4, the sample precipitated, and at pH 10, no endotherm was observed. The endotherm at pH 7 (Fig. 3 *A*, *lowest line*) could be fitted to a two-state mechanism, with $T_m = 332$ K (Table 3).

Structure and stability of EI^{sc} in the presence of the effectors

All the experiments in the presence of PEP and Mg^{2+} were carried out at pH 7, since at this pH the fluorescence intensity was maximal (Fig. 1 *A*) and the fluorescent residues were buried (Table 1). We followed a three-part approach. First, FTIR spectra in the presence of the effectors were acquired and compared with those obtained in their absence to find out whether there were secondary structural changes upon binding. Second, the accessibility of the aromatic residues and structural changes occurring upon binding of the effectors to EI^{sc} was tested by acrylamide quenching experiments and trypsin digestion experiments. And finally, thermal denaturations were carried out to test for changes in protein stability upon binding to the effectors.

Structure of EI^{sc} by FTIR (steady-state measurements)

In Fig. 3 *B*, the amide I′ band of EI^{sc} in the presence of both effectors is shown. The deconvoluted bands in the FTIR spectra suggested that, within the experimental uncertainty, the percentages of secondary structure remained unaltered upon binding of both effectors (Table 4). Similar findings were obtained when any of the effectors was added separately.

Solvent-accessibility of aromatic residues (acrylamide quenching experiments)

Quenching experiments in the presence of the effectors yielded quenching constants in the presence of Mg^{2+} (2.3 ± 0.2 M^{-1} and $\upsilon = 0.5 \pm 0.1$ M^{-1}) similar to those measured in isolated EI^{sc} (Table 1), and smaller when PEP (1.6 ± 0.3 M^{-1} and $\upsilon = 0.5 \pm 0.1$ M^{-1}) or both effectors (1.8 ± 0.2 M^{-1} and $\upsilon = 0.4 \pm 0.2$ M^{-1}) were added.

Trypsin digestion experiments

The digestion patterns in the presence of Mg^{2+} showed the same behavior as in the absence of any effector: most of the protein was rapidly digested within the time of the experiments (*open* and *solid squares*). Conversely, in the presence of PEP (either alone or with Mg^{2+}), the enzyme was more resistant to proteolysis (*open* and *solid circles*) (Fig. 4).

The results of the trypsin digestion and quenching experiments qualitatively agree, indicating that EI^{sc} suffers conformational changes upon binding to PEP. On the other hand, the binding of Mg^{2+} did not alter the structure of the protein.

The stability of EI^{sc} (thermal and calorimetric measurements)

Thermal denaturation experiments in the presence of the effectors were carried out using far-UV CD and FTIR spectroscopies, and DSC measurements (Figs. 2 *C* and 3 *A*)

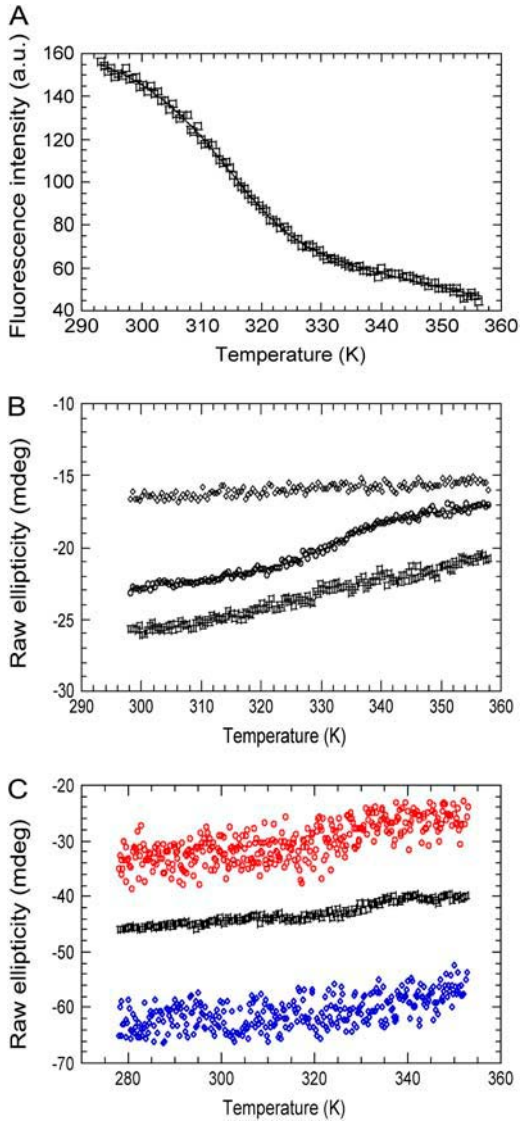

FIGURE 2 Thermal denaturations in the absence and in the presence of the effectors followed by fluorescence and far-UV CD. (*A*) Fluorescence experiments at pH 7 in the absence of effectors, by following the fluorescence intensity at 335 nm after excitation at 295 nm. The line through the data is the fitting to Eqs. 3 and 4. For the sake of clarity, only one-third of the acquired data points have been represented. (*B*) Far-UV CD experiments following the ellipticity at 222 nm: *circles*, pH 9; *squares*, pH 12; *diamonds*, pH 4.0. For the sake of clarity, only half of the acquired data points have been represented. The scale on the *y* axis is arbitrary. The line through the data at pH 9 is the fitting to Eqs. 3 and 4. (*C*) Far-UV CD experiments at pH 7 in the presence of effectors: *red circles*, 5 mM PEP; *black squares*, 2.5 mM Mg^{2+}; and *blue diamonds*, 2.5 mM Mg^{2+} and 5 mM PEP. The scale on the *y* axis is arbitrary.

(Table 3). The addition of PEP slightly destabilized EI^{sc}, and the presence of Mg^{2+} stabilized it. In general, the presence of Mg^{2+}, PEP, or both effectors together had a minor effect on the thermal stability of the protein as judged by the slight changes in T_m (the $\Delta\Delta T_m$s from DSC measurements equal +1.5 K for Mg^{2+}, −1.5 K for PEP, and −0.7 K when both effectors were present).

The EI^{sc} modeled structure

We have modeled the EI^{sc} structure to find a framework in which our experimental results could be adequately explained. Further, this modeled structure will make it possible to explain whether the structures alone can account for the differences in the thermodynamical parameters among the members of the family.

The N-terminal domain showed basically the same structure as the EIN^{ec} (8,9), since the alignments for homology modeling showed only minor deletions in loops between α-helix 1 and α-helix 2, α-helix 2 and α-helix 3, and α-helix 3 and α-helix 4 (Fig. 5 *A*). In essence, the structure consisted of an α-helix subdomain, which is a four-helix bundle, comprising α-helices 1–4; an α/β subdomain, comprising a β-sandwich, formed by a four-stranded parallel β-sheet (β-strands 1−4) and a three-stranded antiparallel β-sheet (β-strands 1, 5, and 6), and three short helices (α-helices 5–7) that contain the phosphorylation site (His^{186}) (Fig. 5 *B*). In the modeled structure, there was a long α-helix that is supposed to serve as a linker to the EIC domain.

The alignment of the C-terminal domain of EI^{sc}, EIC^{sc}, and EIC^{tt} showed a high degree of similarity (>50%) with all the residues in the active center strictly conserved (Fig. 5 *A*).

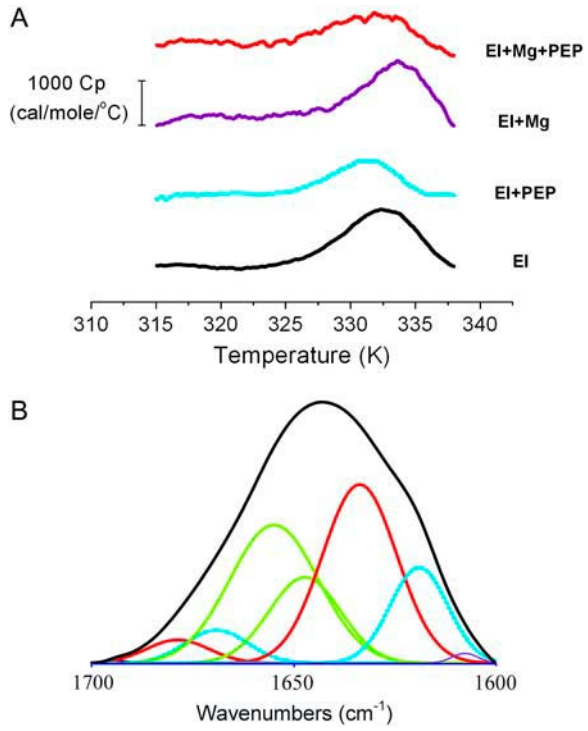

FIGURE 3 Calorimetric (DSC) and spectroscopic (FTIR) experiments of EI^{sc} in the presence of the effectors. (*A*) The concentrations of the effectors were 2.5 mM Mg^{2+} and 5 mM PEP and protein concentration was 1.27 mg/ml, pH 7, in the DSC experiments. (*B*) The deconvoluted bands of the FTIR spectra of EI^{sc} in the presence of 2.5 mM Mg^{2+} and 5 mM PEP corresponding to the percentages of secondary structure: *blue*, β-hairpins and β-turns; *red*, β-sheets; and *green*, α-helices. Experiments were acquired at pH 7, 298 K.

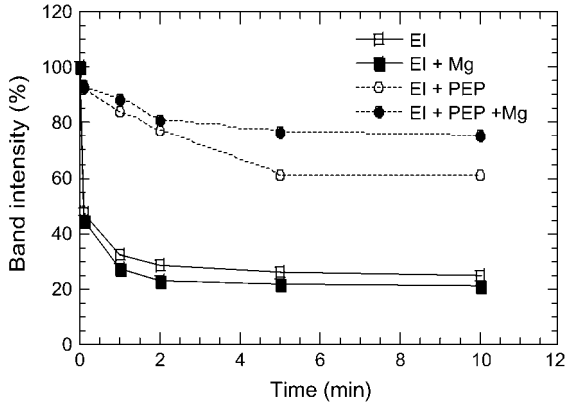

FIGURE 4 Trypsin digestion experiments. Changes in the EI^{sc} intensity band in an SDS-PAGE gel at different times measured from the beginning of the trypsin digestion (concentration rate of EI^{sc}/ trypsin is 500:1). The measurements were repeated three times at any of the different effector concentrations (2.5 mM Mg^{2+} and 5 mM PEP). Experiments were carried out at 298 K.

In essence, the structure of EIC^{sc} was a $\beta 8/\alpha 8$ barrel fold with an additional helix-loop-helix (formed by α-helix 9-α-helix 10) at its C-terminal. This helix-loop-helix motif folded against the barrel, covering a hydrophobic patch (which includes Trp^{461}); the motif was linked to the barrel by two salt bridges, namely, Arg^{537}-Asp^{467} and Arg^{546}-Asp^{459} (Fig. 5 *C*). The modeled structure of the EIC^{sc} monomer differed from that of EIC^{tt} (11) only in a deletion in the loop between α-helix 4 and β-strand 5, which is part of neither the active center nor the dimerization surface.

However, the Fold-X analysis of the modeled EIC^{sc} dimer showed differences in the stability and in the interaction energy when compared to those of EIC^{tt} (11). Similarly to that observed for EIC^{ec}, the electrostatic, as well as the van der Waals interactions, were decreased in EIC^{sc}, losing several salt bridges and hydrogen bonds when compared with the structure of EIC^{tt}. The helix-loop-helix motif formed by the α-helix 9-α-helix 10 shows intermonomer salt bridges: Asp^{540} in the motif with $Arg^{422\prime}$ in α-helix 5 from the other monomer (the prime is used to designate residues in the other monomer). The dimerization surface included several salt-bridge networks, such as Asp^{467}-$Arg^{424\prime}$, Arg^{456}-$Asp^{358\prime}$, Asp^{540}-$Arg^{422\prime}$, Asn^{345}-$Asp^{448\prime}$, as well as backbone-backbone hydrogen bonds (Fig. 5 *C*). When compared with the EIC^{tt}, the dimeric surface was losing hydrogen bonds (which yielded $\Delta\Delta G = +5.42$ kcal mol^{-1}) and hydrophobic contacts ($\Delta\Delta G = +4.72$ kcal mol^{-1}), making the monomer-monomer interaction less stable. These differences could be due to the thermophilic nature of EIC^{tt}.

The structure of the modeled dimer nicely explained why the solvent accessibility of the Trp^{461} was reduced as the concentration of EI^{sc} increased (see before). Upon dimer formation, the higher part of the groove, formed by the helix-loop-helix motif and the rest of the protein (and which traps Trp^{461}), was partly fixed by the other monomer via several salt bridges, thus hampering solvent-accessibility to the indole moiety.

We attempted, by docking of the EIN^{sc} and EIC^{sc} domains, to model the whole structure of EI^{sc}, trying to keep the active-site histidine (in the EIN^{sc} domain) close to the PEP binding site (in the EIC^{sc} domain). Our models were in all cases (500 runs) unsuccessful, since the distance between both sites was very large to allow for the transference of the phosphate group (>10 Å). This result was also reported in a study of docking of EIC^{tt} with EIN^{ec} (11), and suggests that the structure of some, if not both, domains should be different in the intact EI^{sc} from in the isolated domains.

DISCUSSION

Structure of EI^{sc} in the absence of effectors

We carried out studies at different pH using several spectroscopic probes to test whether the structure of EI^{sc} changed. To the best of our knowledge these are the first studies of this kind carried out in any member of the EI family. Between pH 6 and 8, the tertiary structure of EI^{sc} remained unaltered, as suggested by fluorescence and ANS-binding (Fig. 1 *A*); however, there were changes in the secondary structure, as reported by CD (Fig. 1 *C*). These changes were probably due to a histidine residue, which titrates in that pH region (43). Inspection of the EIC^{sc} (Fig. 5 *C*) and EIN^{sc} structures (Fig. 5 *B*) indicates that: 1), all histidine residues were solvent-exposed; and, 2), no histidine residue was near to any of the tyrosine residues or Trp^{461}. Based on these findings, it is tempting to suggest that the changes monitored by far-UV CD were due to the proximity of residues in the tertiary structure of the whole intact EI^{sc} structure, but not of the isolated domains (and then, in those modeled in this work). These findings seem to support the hypothesis that both domains must suffer large conformational rearrangements when they are joined. Interestingly enough, based on DSC experiments and the different stabilities of the EIN^{ec} and EI^{ec}, interactions between EIN and EIC in the whole intact EI have been suggested (44). However, we cannot rule out that an alternative explanation to the titration curve is that the deprotonation of a histidine residue can be felt by a residue(s) far enough in the three-dimensional structure (see Fersht (45) and references therein) affecting its (their) environment(s).

Above pH 8, the intensity of the fluorescence spectra decreased (Fig. 1 *A*) and the maximum wavelength of the emission spectra moved toward higher values (data not shown), indicating solvent exposure of the fluorescence residues. Furthermore, the K_{sv} values were higher than those measured at neutral pH but smaller than those at acidic pH and in 7 M GdmHCl (Table 1). However, the molar ellipticity at 222 nm at basic pH was larger (in absolute value) than that at pH 7.0 (Fig. 1 *C*), thus indicating that the helical content of EI^{sc} increased. This increase in the helicity was further confirmed

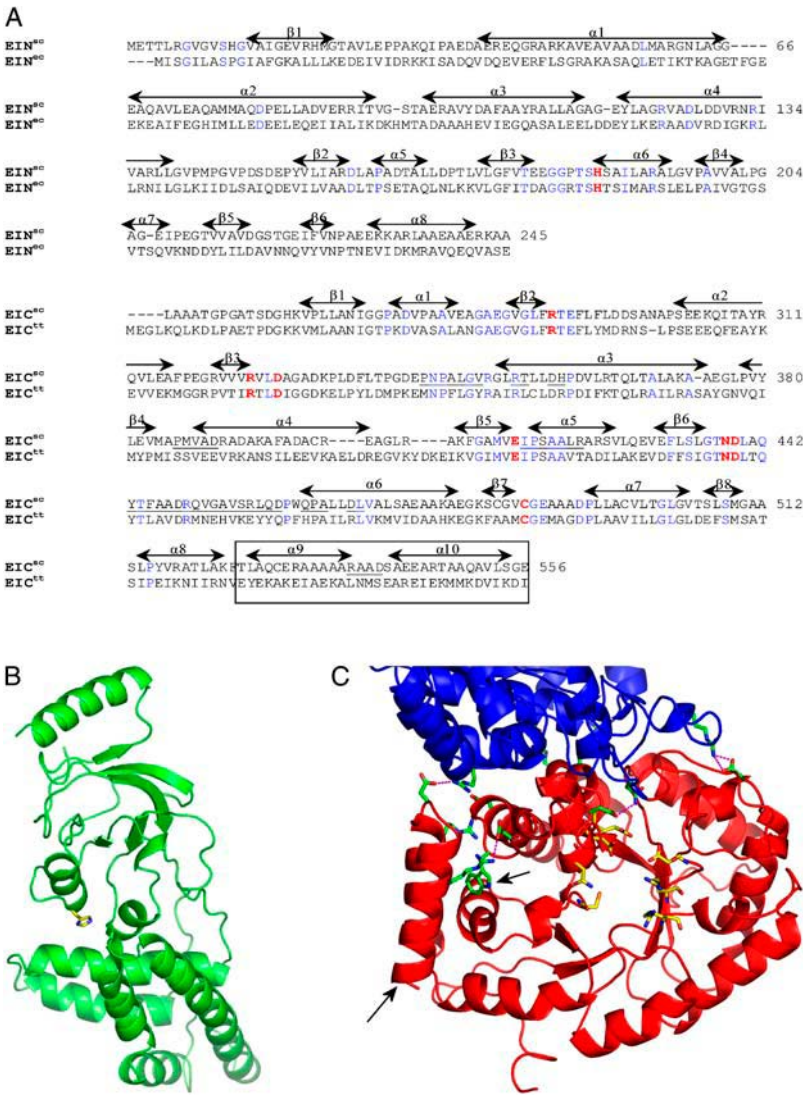

FIGURE 5 Alignments and modeled structure of EI^{sc}. (*A*) Aligned sequences of EIN^{sc} and EIN^{ec} (*upper*), and EIC^{sc} and EIC^{tt} (*lower*). Residues in red denote the phosphorylation site (N-terminal) and the residues involved in the active center (C-terminal); residues in blue are conserved residues among species in multiple sequence alignments (data not shown). Underlined regions denote residues involved in the C-terminal dimerization surface. The boxed area highlights the helix-loop-helix motif located at the C-terminal of EI^{sc}. (*B*) Modeled structure of EIN^{sc} showing the α subdomain (*lower*) and α/β subdomain (*upper*). The residue in yellow (His^{186}) is the phosphorylation site. (*C*) Detail of the EIC^{sc} dimeric model: the $\beta 8/\alpha 8$ barrel ends with a helix-loop-helix at the C-terminal of the domain (*left arrow*) that occludes Trp^{461} (*right arrow*). Residues in green form the most important salt bridges and hydrogen bonds (*magenta*) upon dimerization. Two additional salt bridges lock the helix-loop-helix motif to the barrel. Residues in yellow indicate the phosphorylation site.

by the FTIR experiments carried out at pH 10 (Table 2). Taken together, these data suggest that there were structural changes, which partially solvent-exposed the indole moiety and/or tyrosine residues, and modified the ellipticity at 222 nm (41,42).

On the other hand, at acidic pH, EI^{sc} lost its tertiary structure and solvent-exposed hydrophobic patches, as suggested by 1), the changes in the fluorescence intensity (Fig. 1 *A*, *open squares*); 2), the ANS-binding experiments (Fig. 1 *A*, *solid squares*); 3), the changes in solvent accessibility (Table 1); and 4), the absence of a sigmoidal thermal transition at low pH (Fig. 2 *B*). Although there were changes in the tertiary structure, EI^{sc} retained some, if not all, of its secondary structure, as shown by the increase (in absolute value) of the [Θ] at 222 nm (Fig. 1 *C*) and the FTIR data acquired at pH 3 (Table 2). Furthermore, the shape of the CD spectrum was altered between pH 3.0 and 5.5 (Fig. 1 *B*) at wavelengths ~208 nm. Changes in the CD signal at 208 nm (where the parallel polarized π-π* transition occurs) are the result of a flexibility of the structure (46). The pK_a leading to the acidic species could be determined from the ANS-binding and intrinsic fluorescence measurements, suggesting that one aspartic and/or glutamic acid must be responsible for this transition (43). These features (namely, the absence of tertiary structure, the lack of a sigmoidal behavior in thermal heating, solvent-exposure of hydrophobic residues, and a large amount of secondary structure) are characteristic of the so-called molten-globule species (47,48). It can be concluded, then, that EI^{sc} at low pH unfolded via a molten-globule-like species, as it has been described in other large multimeric proteins (49). It is tempting to suggest, based on our results, that the species populated at high pH is also a molten-globule-like species, although it did not bind ANS (Fig. 1 *A*).

The biological relevance of the partially folded species at acidic pH is unknown, and we do not know whether the residual secondary structure detected by CD and FTIR (Table 2) was native-like. We can speculate, however, based on the

TABLE 2 Secondary structural analysis of EI^{sc} as determined by FTIR at different pHs

Wavenumber (cm^{-1})	Structural assignment*	pH 3	pH 7†	pH 8.5	pH 10
1693	β-hairpin (64)	0.2	0.2	0.1	0.4
1679	turn/loop/(0, π) β-sheet (63)	2.7	2.7	2.4	3.0
1668	β-turn (66)	4.0	12.4	10.8	13.1
1657	loops/α-helix (63,65)	50.9‡	9.3	15.6	35.6
1648	disordered structure/α-helix (63,65)	—	35.2	24.7	19.4
1633	antiparallel β-sheet (63)	33.9	29.4	37.0	25.4
1620	β-hairpin (64)	8.3	10.8	9.4	3.1

Errors in the percentages of secondary structure are estimated to be ±10%.
*There is one more band, which has not been indicated in Table 2, centered at 1606 cm^{-1}. This band is assigned to side chains (64) and accounts for 0.2% of the whole area of the amide I′ band in EI at any pH.
†Data for pH 7 are from Hurtado-Gómez et al. (23), and are presented for purposes of comparison.
‡At this pH, the deconvolution procedures yielded a single band centered at 1650 cm^{-1}.

modeled three-dimensional structure of the EIC^{sc}, that the large amphipathic surface in the dimer interface could be exposed to solvent upon monomer formation; furthermore, there is a network of aspartic residues involved in salt bridges at the dimeric interface (Fig. 5 *C*). The partial solvent exposure of this hydrophobic surface (due to protonation of some aspartic residue) could then cause binding to ANS, and thus the molten-globule of EI^{sc} could have some of its dimeric interface partially disrupted. However, our experimental observations at low pH also can be explained, for instance, by the solvent exposure of the helix-loop-helix formed by α-helix 9 and α-helix 10, whose movement from the rest of the protein would expose a large hydrophobic surface able to bind ANS, and would alter the fluorescence of Trp^{461} (Fig. 1 *A*, *open squares*). To test this hypothesis, we carried out thermal denaturation experiments followed by the fluorescence of ANS at three different pH (2.0, 3.5, and 8.0) and in all cases, the intensity of the fluorescence at 480 nm was very high at low temperatures (between 288 and 293 K), but decreased as the temperature was raised (data not shown). However, the absence of native baseline at low temperatures did not yield reliable results when fitting the data to Eq. 4.

Folding and stability of EI^{sc} in the absence of effectors

Two unfolding mechanisms have been described in oligomeric proteins exposed to high temperatures or high concentrations of chemical denaturants at equilibrium (49–51): 1), dissociation followed by unfolding of the native or partially unfolded monomeric species; and 2), denaturation without the accumulation of the native dissociated species. In this work, between pH 6 and 8, EI^{sc} was a well-folded dimer that could be heat-denatured in a single sigmoidal transition, and thus it followed the second mechanism proposed. All the thermal and the calorimetric transitions were reversible and they could be fitted to a two-state model (Table 3).

Converse to observations in other EI proteins by DSC (6) and CD (52), the DSC experiments with EI^{sc} did not show two transitions. In the EI protein from *Salmonella typhimurium*, EI^{st}, the DSC scans show a single peak between pH 6.5 and 7 (6), due to simultaneous unfolding between the C- and N-terminal domains. This simultaneous unfolding is strongly pH-dependent, and at high pH, two peaks with different thermodynamical properties are observed, one corresponding to EIN (with pH-independent T_m values) and a second corresponding to EIC (with pH-dependent T_m-values) (6). Interestingly enough, two peaks also appear in the unfolding of EI^{ec} (4). In EI^{sc}, a single peak was observed in CD and DSC experiments, but in the pH range where the thermal transitions could be followed (pH 7–9), two different peaks were not observed; further, the T_m of the sole transition observed was pH-independent between pH 7 and 9 (Fig. 2 *B*). As the EIN^{st} and EIN^{ec} have pH-independent T_m values close to 328 K (4,5), and thus similar to the T_m value measured in EI^{sc} (Table 2), it is tempting to suggest that the sole peak observed in the thermal scans of EI^{sc} was due to the EIN^{sc}.

TABLE 3 Thermodynamic parameters for thermal unfolding of EI^{sc}

	Technique					
	FTIR		Far-UV CD		DSC*	
Effector(s) present	T_m (K)	Scan rate (K/h)	T_m (K)	Scan rate (K/h)	T_m (K)	Scan rate (K/h)
EI†	332.1 ± 0.9	30	329.9 ± 0.4	60	332.27 ± 0.04	90
PEP	329.0 ± 0.5	30	326.4 ± 0.7	60	330.81 ± 0.03	90
Mg^{2+}	329 ± 2	30	331.5 ± 0.8	60	333.57 ± 0.03	90
PEP + Mg^{2+}	330.0 ± 0.4	30	–‡	60	331.58 ± 0.07	90

Protein concentrations were: 44.7 mg/ml in the FTIR experiments, 0.254 mg/ml in CD spectra, and 1.27 mg/ml in DSC measurements at pH 7.
*Thermodynamic parameters were obtained from deconvolutions of DSC data to a two-state model. Proteins were equilibrated in 10 mM Hepes, pH 7, 10 mM NaCl, and 2 mM β-mercaptoethanol.
†In the case of EI, no effectors were present.
‡The thermal denaturation with PEP + Mg^{2+} could not be determined with far-UV CD due to the poor signal/noise ratio (Fig. 3 *A*, *upper*).

TABLE 4 Secondary structural analysis of EI^{sc} as determined by FTIR

Wavenumber (cm^{-1})	Structural assignment*	EI†	EI + Mg^{2+}	EI + PEP	EI + Mg^{2+} + PEP
1693	β-hairpin	0.2	0.1	0.3	0.1
1679	turn/loop/(0, π) β-sheet	2.7	3.3	2.0	3.1
1668	β-turn	12.4	4.7	14.4	3.3
1657	loops/α-helix	9.3	12.7	5.4	7.1
1648	disordered structure/α-helix	35.2	32	29.4	37.0
1633	antiparallel β-sheet	29.4	37.6	41.4	31.4
1620	β-hairpin	10.8	8.8	6.3	10.0

Errors in the percentages of secondary structure are estimated to be $\pm 10\%$.
*There is one more band, which has not been indicated in Table 4, centered at 1606 cm^{-1}. This band is assigned to side chains (64) and accounts for 0.2% of the whole area of the amide I′ band in EI alone, 0.8% for EI + Mg^{2+}, 0.3% for EI + PEP, and 8% for EI + Mg^{2+} + PEP.
†EI data are from Hurtado-Gómez et al. (23), and are presented for purposes of comparison.

This different behavior in the thermograms among the members of a protein family is not new, and it has been reported, for instance, in the thermodynamic unfolding of dimeric histone-like proteins (53).

An estimation of the T_m of EIC^{sc}, based on the fluorescence results (Fig. 2 *A*), was also obtained. This value (311 $\pm$ 5 K, at 4 μM protein concentration, 315 $\pm$ 9 K, at 6 μM protein concentration) was similar, within the experimental uncertainty, to that obtained in the intact EI^{ec} (4), where two tryptophan residues are located at the C-terminal region of the protein. The absence of a long native baseline at this and other pH in EI^{sc} precluded any reliable conclusion on the pH independence of this value of T_m.

We carried out measurements at different protein concentrations either by CD and fluorescence in the concentration range 4–8 μM at pH 7. The transitions measured by CD became broader as the concentration increased, and although a small increase was observed when the concentration was raised (3 μM yielded $T_m = 328.8 \pm 0.2$ K; 4 μM, $T_m = 329.9 \pm 0.4$ K (Table 1); and 8 μM, $T_m = 330.5 \pm 0.6$ K), all the measurements are within experimental error, and the differences are probably due to the broadness of the transition. The fact that the CD thermal transitions of EI^{sc} became broad as the concentration was increased suggests that the thermal transition of the EIC^{sc} is also being observed, as happens in EI^{ec} (52). Either we could not unambiguously determine the protein-concentration independence of the thermal midpoint from fluorescence measurements (see above, for the values, and Fig. 2 *A*), since the native baselines showed large slopes, probably due to thermoquenching of the tryptophan (26), leading to large fitting errors. In EI^{ec}, the thermal midpoint of the transition monitored by fluorescence is concentration-dependent (52), but the slopes of the native baseline are smaller due to the fact that two tryptophan residues are observed in the C-terminus of EI^{ec}.

Structure and stability of EI^{sc} in the presence of effectors

The addition of the effectors to EI^{sc} did not alter substantially the secondary structure of the protein, as shown by FTIR (Table 4). Similar results have been observed in 1), the enzyme malate synthase G (54), a close structural analog of pyruvate dikinase and EIC (11), where binding to pyruvate does not cause large structural changes (55); and 2), the pyruvate dikinase from maize, where only small changes are observed in selected regions upon binding of PEP (56). These small changes upon binding of the effectors were also monitored by the changes in the accessibility of fluorescent residues and the trypsin digestion patterns. Upon binding, the accessibilities of the fluorescent residues, when compared to those in EI^{sc} alone, were decreased in the presence of PEP (either alone or with Mg^{2+}), and remained unaltered in the presence of Mg^{2+} alone. Furthermore, trypsin digestion was reduced in the presence of PEP (either alone or with Mg^{2+}), but not in the presence of Mg^{2+} alone. Taken together, both results suggest the presence of small conformational changes, which otherwise are not detected by FTIR (Table 4), when PEP was bound to EI^{sc}. These changes led to burial of the Trp and/or Tyr and other regions susceptible to trypsin digestion.

The presence of Mg^{2+} slightly increased the T_m of EI^{sc} alone, probably due to formation of an octahedral-coordination-geometry complex to the native state of EI^{sc}, as occurs in other homologous proteins (56,57). The addition of PEP alone slightly destabilized the protein (Table 3), suggesting that the conformational changes monitored by trypsin digestion and quenching experiments did not result in large thermodynamic variations. Interestingly enough, the addition of both effectors to EI^{sc} partially compensated for the stabilizing effect of Mg^{2+}. We hypothesize that this compensatory effect could be due to a change in the coordination sphere of the Mg^{2+} by directly involving the phosphoryl group of the PEP moiety, as it occurs in a member of the pyruvate dikinase family (57).

Thermodynamic and folding properties versus structure among the members of a protein family

Early studies suggested that folding and equilibrium pathways of homologous proteins were similar, and that the folding of a certain structure was thus conserved through evolution (58,59). However, there are examples of homologous proteins that unfold following different patterns and, in addition, have different thermodynamical parameters (60,61). In EI^{sc}, although its sequence homology and its structure are similar to those of other EI proteins, the calorimetric equilibrium unfolding, as shown by DSC, is different. These changes in the thermodynamical parameters point to subtle conformational variations in the packing of some residues. The differences among the modeled structure and that of

EIC^{tt} in the hydrogen-bond pattern, and the van der Waals contacts in the dimerization interface could explain those changes. At the moment, however, we do not know whether these small changes in the structure are also responsible for the observed considerable specificity of the phosphotransfer reaction between EI and HPr among the different species and the differences in their enthalpic variations in their binding reactions (45,62).

A similar reasoning can be used to explain the outcome of the effectors. The secondary structure of EI^{sc} upon binding was not largely affected (Table 4), but there were subtle changes in the stability of the protein (Table 3), which suggest that small rearrangements occurred upon binding, as further confirmed by quenching fluorescence and trypsin digestion experiments.

We thank María Francisca Lozano for her involvement in the early stages of this work and Francisco N. Barrera for critical reading of the manuscript and helpful suggestions. We gratefully thank María T. Garzón, May García, María C. Fuster, Helena López, Eva Martínez, and Javier Casanova for excellent technical assistance. We deeply thank both reviewers for their criticisms, ideas, and suggestions.

This work was supported by Projects CTQ2004-07716 from the Spanish Ministerio de Educación y Ciencia (MEC) to J.G., and Projects GV04B-402 from Generalitat Valenciana, and CTQ2004-04474 and CTQ2005-00360/BQU from MEC, to J.L.N. F.T. and H.N. were supported by grant SFB473 of the Deutsche Forschungsgemeinschaft. E.H.G. is a recipient of a predoctoral fellowship from Generalitat Valenciana.

REFERENCES

1. Postma, P. W., J. Lengeler, and G. R. Jacobson. 1993. Phosphoenolpyruvate carbohydrate phosphotransferase systems of bacteria. *Microbiol. Rev.* 57:543–594.
2. Dimitrova, M. N., A. Peterkofsky, and A. Ginsburg. 2003. Opposing effects of phosphoenolpyruvate and pyruvate with Mg^{2+} on the conformational stability and dimerization of phosphotransferase enzyme I from *Escherichia coli*. *Protein Sci.* 12:2047–2056.
3. Chauvin, F., L. Brand, and S. Roseman. 1994. Sugar transport by the bacterial phosphotransferase system. Studies on the molecular weight and association of Enzyme I. Characterization of the *Escherichia coli* enzyme I monomer/dimer transition kinetics by fluorescence anisotropy. *J. Biol. Chem.* 269:20270–20274.
4. Dimitrova, M. N., R. H. Szczepanowski, S. B. Ruvinov, A. Peterkofsky, and A. Ginsburg. 2002. Interdomain interaction and substrate coupling effects of dimerization and conformational stability of Enzyme I of the *Escherichia coli* phosphoenolpyruvate:sugar phosphotransferase system. *Biochemistry.* 41:906–913.
5. Lux, R., K. Jahreis, K. Bettenbrock, J. S. Parkinson, and J. W. Lengeler. 1995. Coupling the phosphotransferase system and the methyl-accepting chemotaxis protein-dependent chemotaxis signaling pathways of *Escherichia coli*. *Proc. Natl. Acad. Sci. USA.* 92:11583–11587.
6. LiCalsi, C., T. S. Crocenzi, E. Freire, and S. Roseman. 1991. Sugar transport by the bacterial phosphotransferase system. Structural and thermodynamics domains of Enzyme I of *Salmonella typhimurium*. *J. Biol. Chem.* 266: 19519–19527.
7. Lee, B. R., P. Lecchi, L. Panell, H. Jaffe, and A. Peterkofsky. 1994. Identification of the N-terminal domain of enzyme I of the *Escherichia coli* phosphoenolpyruvate:sugar phosphotransferase system produced by proteolytic digestion. *Arch. Biochem. Biophys.* 312:121–124.
8. Liao, D. I., E. Silverton, Y. J. Seok, B. R. Lee, A. Peterkofsky, and D. R. Davies. 1996. The first step in sugar transport: crystal structure of the amino terminal domain of enzyme I of the *E. coli* PEP:sugar phosphotransferase system and a model of the phosphotransfer complex with HPr. *Structure.* 4:861–872.
9. Garret, D. S., Y. J. Seok, D. I. Liao, A. Peterkofsky, A. M. Gronenborg, and G. M. Clore. 1997. Solution structure of the 30 kDa N-terminal domain of enzyme I of the *Escherichia coli* phosphoenolpyruvate:sugar phosphotransferase system by multidimensional NMR. *Biochemistry.* 36:2517–2530.
10. Garret, D. S., Y. J. Seok, A. Peterkofsky, A. M. Gronenborg, and G. M. Clore. 1999. Solution structure of the 40,000 M_r phosphoryl transfer complex between the N-terminal domain of enzyme I and HPr. *Nat. Struct. Biol.* 6:166–173.
11. Oberholzer, A. E., M. Bumann, P. Schneider, C. Bächler, C. Siebold, U. Baumann, and B. Erni. 2005. Crystal structure of the phosphoenolpyruvate-binding enzyme I domain from the *Thermoanaerobacter tengcongensis* PEP:sugar phosphotransferase system. *J. Mol. Biol.* 346:521–532.
12. Seok, Y. J., B. R. Lee, P. P. Zhu, and A. Peterkofsky. 1996. Importance of the carboxyl-terminal domain of enzyme I of the *Escherichia coli* phosphoenolpyruvate:sugar phosphotransferase system for phosphoryl donor specificity. *Proc. Natl. Acad. Sci. USA.* 93:347–351.
13. Bentley, S. D., K. F. Chater, A. M. Cerdeno-Tarraga, G. L. Challis, N. R. Thomson, K. D. James, D. E. Harris, M. A. Quail, H. Kieser, D. Harper, A. Bateman, S. Brown, et al. 2002. Complete genome sequence of the model actinomycete *Streptomyces coelicolor* A3(2). *Nature.* 417:141–147.
14. Titgemeyer, F., J. Walkenhorst, X. Cui, J. Reizer, and M. H. Jr. Saier. 1994. Proteins of the phosphoenolpyruvate:sugar phosphotransferase system in *Streptomyces*: possible involvement in the regulation of antibiotic production. *Res. Microbiol.* 145:89–92.
15. Nothaft, H., D. Dresel, A. Willimek, K. Mahr, M. Niederweis, and F. Titgemeyer. 2003. The phosphotransferase system of *Streptomyces coelicolor* is biased for N-acetylglucosamine metabolism. *J. Bacteriol.* 185:7019–7023.
16. Parche, S., R. Schmid, and F. Titgemeyer. 1999. The PTS system of *Streptomyces coelicolor*: identification and biochemical analysis of a histidine phosphocarrier protein HPr encoded by the gene ptsH. *Eur. J. Biochem.* 265:308–317.
17. Fernandez-Ballester, G., J. Maya, A. Martin, S. Parche, J. Gomez, F. Titgemeyer, and J. L. Neira. 2003. The histidine-phosphocarrier protein of *Streptomyces coelicolor* folds by a partially folded species at low pH. *Eur. J. Biochem.* 270:2254–2267.
18. Neira, J. L., and J. Gomez. 2004. The conformational stability of the *Streptomyces coelicolor* histidine-phosphocarrier protein. Characterization of cold denaturation and urea-protein interactions. *Eur. J. Biochem.* 271:2165–2181.
19. Azuaga, A. I., J. L. Neira, and N. A. van Nuland. 2005. HPr as a model protein in structure, interaction, folding and stability studies. *Protein Pept. Lett.* 12:123–137.
20. Butler, M. J., J. Deutscher, P. W. Postma, T. J. Wilson, A. Galinier, and M. J. Bibb. 1999. Analysis of a ptsH homologue from Streptomyces coelicolor A3(2). *FEMS Microbiol. Lett.* 177:279–288.
21. Jones, B. E., V. Dossonet, E. Küster, W. Hillen, J. Deutscher, and R. E. Klevit. 1997. Binding of the catabolite repressor protein to its DNA target is regulated by phopshorylation of its co-repressor HPr. *J. Biol. Chem.* 272:26530–26535.
22. Gunasekaran, G., S. J. Eyles, A. T. Haggler, and L. M. Gierasch. 2001. Keeping it in the family: folding studies of related proteins. *Curr. Opin. Struct. Biol.* 11:83–93.
23. Hurtado-Gómez, E., F. N. Barrera, and J. L. Neira. 2005. Structure and conformational stability of the enzyme I of *Streptomyces coelicolor* explored by FTIR and circular dichroism. *Biophys. Chem.* 115:229–233.
24. Pace, C. N., and J. M. Scholtz. 1997. Measuring the conformational stability of a protein. *In* Protein Structure, 2nd ed. T. E. Creighton, editor. Oxford University Press, Oxford, UK. 253–259.
25. Mann, C. J., and C. R. Matthews. 1993. Structure and stability of an early folding intermediate of *Escherichia coli* Trp aporepressor

measured by far-UV stopped-flow circular dichroism and 8-anilino-1-naphthalene sulfonate binding. *Biochemistry.* 32:5282–5290.

26. Lakowicz, J. R. 1999. Principles of Fluorescence Spectroscopy, 2nd ed. Plenum Press, New York.
27. Sipos, T., and J. R. Merkel. 1970. An effect of calcium ions on the activity, heat, stability and structure of trypsin. *Biochemistry.* 9:2766–2775.
28. Haris, P. I., G. T. Robillard, A. A. van Dik, and D. Chapman. 1992. Potential of ^{13}C and ^{15}N labelling for studying protein-protein interaction using Fourier transform infrared spectroscopy. *Biochemistry.* 31:6279–6284.
29. Jackson, M., and H. H. Mantsch. 1995. The use and misuse of FTIR spectroscopy in the determination of protein structure. *Crit. Rev. Biochem. Mol. Biol.* 30:95–120.
30. Arrondo, J. L. R., and F. M. Goñi. 1999. Structure and dynamics of membrane proteins as studied by infrared spectroscopy. *Prog. Biophys. Mol. Biol.* 72:367–405.
31. Barth, A., and C. Zscherp. 2002. What vibrations tell us about proteins. *Q. Rev. Biophys.* 35:369–430.
32. Backmann, J., G. Schäfer, L. Wyns, and H. Bönisch. 1998. Thermodynamics and kinetics of unfolding of the thermostable trimeric adenylate kinase from the archeon *Sulfolobus acidocaldarius*. *J. Mol. Biol.* 284:817–833.
33. Schwede, T., J. Kopp, N. Guex, and M. C. Peitsch. 2003. SWISS-MODEL: an automated protein homology-modelling server. *Nucleic Acids Res.* 31:3381–3385.
34. Guex, N., and M. C. Peitsch. 1997. SWISS-MODEL and the Swiss-PDB viewer: an environment for comparative protein modelling. *Electrophoresis.* 18:2714–2723.
35. Guerois, R., J. E. Nielsen, and L. Serrano. 2002. Predicting changes in the stability of proteins and protein complexes: a study of more than 1000 mutations. *J. Mol. Biol.* 320:369–387.
36. Schymkowitz, J., J. Borg, F. Stricher, R. Nys, F. Rousseau, and L. Serrano. 2005. The FoldX web server: an online force field. *Nucleic Acids Res.* 33:W382–W388.
37. Laskowski, R., J. Rullmann, M. MacArthur, R. Kaptein, and J. M. Thornton. 1996. AQUA and PROCHECK-NMR: programs for checking the quality of protein structures solved by NMR. *J. Biomol. NMR.* 8:477–486.
38. DeLano, W. L. 2002. The PyMOL Molecular Graphics System DeLano Scientific LLC, San Carlos, CA. PyMOL molecular graphics system on World Wide Web URL: http://www.pymol.org.
39. Semisotnov, G. V., N. A. Rodionova, O. I. Razgulyaev, V. N. Uversky, A. F. Gripas, and R. I. Gimanshin. 1991. Study of the ''molten globule'' intermediate state in protein folding by a hydrophobic fluorescent probe. *Biopolymers.* 31:119–128.
40. Stryer, L. 1965. The interaction of a naphthalene sulfonate dye with apomyoglobin and apohemoglobin: a fluorescent probe of non-polar binding site. *J. Mol. Biol.* 13:482–495.
41. Woody, R. W. 1995. Circular dichroism. *Methods Enzymol.* 246:34–71.
42. Kelly, S. M., and N. C. Price. 2000. The use of circular dichroism in the investigation of protein structure and function. *Curr. Protein Pept. Sci.* 1:349–384.
43. Cantor, C. R., and P. R. Schimmel. 1980. Biophysical Chemistry. W. H. Freeman, New York.
44. Zhu, P. P., R. H. Szczepanowski, N. J. Nosworthy, A. Ginsburg, and A. Peterkofsky. 1999. Reconstitution studies using the helical and carboxyl-terminal domains of enzyme I of the phosphoenolpyruvate: sugar phosphotransferase system. *Biochemistry.* 38:15470–15479.
45. Fersht, A. R. 1999. Structure and Mechanism in Protein Science. A Guide to Enzyme Catalysis and Protein Folding. W. H. Freeman, New York.
46. Chin, D. R., R. W. Woody, C. A. Rohl, and R. L. Baldwin. 2002. Circular dichroism spectra of short, fixed-nucleus alanine helices. *Proc. Natl. Acad. Sci. USA.* 99:15416–15421.
47. Ptitsyn, O. B. 1995. Molten globule and protein folding. *Adv. Protein Chem.* 47:83–229.
48. Fink, A. L. 1995. Compact intermediate states in protein folding. *Annu. Rev. Biophys. Biomol. Struct.* 24:495–522.
49. Jaenicke, R., and H. Lilie. 2000. Folding and association of oligomeric and multimeric proteins. *Adv. Protein Chem.* 53:329–401.
50. Neet, K. E., and D. E. Timm. 1994. Conformational stability of dimeric proteins: quantitative studies by equilibrium denaturation. *Protein Sci.* 3:2167–2174.
51. Mok, Y. K., G. de Prat Gay, P. J. Butler, and M. Bycroft. 1996. Equilibrium dissociation and unfolding of the dimeric human papillomavirus strain 16 E2 DNA binding protein. *Protein Sci.* 5:310–319.
52. Nosworthy, N. J., A. Peterkofsky, S. König, Y.-J. Seok, R. H. Szczepanowski, and A. Ginsburg. 1998. Phophorylation destabilizes the amino-terminal domain of enzyme I of the *Escherichia coli* phosphoenolpyruvate:sugar phosphotransferase system. *Biochemistry.* 37: 6718–6726.
53. Ramstein, J., N. Hrvouet, F. Coste, C. Zelwer, J. Oberto, and B. Castaing. 2003. Evidence of a thermal unfolding dimeric intermediate for the *Escherichia coli* histone-like HU proteins: thermodynamics and structure. *J. Mol. Biol.* 331:101–121.
54. Howard, B. R., J. A. Endrizzi, and S. J. Remington. 2000. Crystal structure of *Escherichia coli* malate synthase G complexed with magnesium and glyoxylate at 2.0 A resolution: mechanistic implications. *Biochemistry.* 39:3156–3168.
55. Tugarinov, V., and L. E. Kay. 2003. Quantitative NMR studies of high molecular weight proteins: application to domain orientation and ligand binding in the 723 residue enzyme malate synthase G. *J. Mol. Biol.* 327:1121–1133.
56. Nakanishi, T., T. Nakatsu, M. Matsuoka, K. Sakata, and H. Kato. 2005. Crystal structures of pyruvate phosphate dikinase from maize revealed an alternative conformation in the swivelling-domain motion. *Biochemistry.* 44:1136–1144.
57. Herzberg, O., C. C. H. Chen, S. Liu, A. Tempczyk, A. Howard, M. Wei, D. Ye, and D. Dunaway-Mariano. 2002. Pyruvate site of pyruvate phosphate dikinase: crystal structure of the enzyme-phosphonopyruvate complex, and mutant analysis. *Biochemistry.* 41:780–787.
58. Kragelund, B. B., P. Hojrup, M. S. Jensen, C. K. Schejerling, E. Juul, J. Knudsen, and F. M. Poulsen. 1996. Fast and one-step folding of closely and distant related homologous proteins of a four-helix bundle family. *J. Mol. Biol.* 256:187–200.
59. Hollecker, M., and T. E. Creighton. 1983. Evolutionary conservation and variation of protein folding pathways. Two protease inhibitor homologues from black mamba venom. *J. Mol. Biol.* 168:409–437.
60. Chánez-Cárdenas, M. E., G. Pérez-Hernández, B. G. Sánchez-Rebollar, M. Costas, and E. Vázquez-Contreras. 2005. Reversible equilibrium unfolding of triosephosphate isomerase from *Trypanosoma cruzi* in guanidinium hydrochloride involves stable dimeric and monomeric intermediates. *Biochemistry.* 44:10883–10892.
61. Fitter, J., and S. Haber-Pohlmeier. 2004. Structural stability and unfolding properties of thermostable bacterial α-amylases: a comparative study of homologous enzymes. *Biochemistry.* 43:9589–9599.
62. Reizer, J., S. L. Sutrina, L. F. Wu, J. Deutscher, P. Reddy, and M. H. Jr. Saier. 1992. Functional interactions between proteins of the phosphoenolpyruvate:sugar phosphotransferase systems of *Bacillus subtilis* and *Escherichia coli*. *J. Biol. Chem.* 267:9158–9169.
63. Surewicz, W. K., and H. H. Mantsch. 1988. New insight into protein secondary structure from resolution-enhanced infrared spectra. *Biochim. Biophys. Acta.* 952:115–130.
64. Arrondo, J. L., F. J. Blanco, L. Serrano, and F. M. Goñi. 1996. Infrared evidence of a β-hairpin peptide structure in solution. *FEBS Lett.* 384:35–37.
65. Denning, D. P., V. N. Uversky, S. S. Patel, A. L. Fink, and M. Rexach. 2002. The *Saccharomyces cerevisiae* nucleoporin Nup2p is a natively unfolded protein. *J. Biol. Chem.* 277:33447–33455.
66. Chechín, R., I. Iloro, M. J. Marcos, E. Villar, V. L. Shnyrov, and J. L. Arrondo. 1999. Thermal and conformational changes of a β-sheet protein monitored by infrared spectroscopy. *Biochemistry.* 38:1525–1530.